Carbon 101 (2016) 159–167

Contents lists available at ScienceDirect

Carbon

journal homepage: www.elsevier.com/locate/carbon

Fabrication and properties of carbon nanotube-reinforced hydroxyapatite composites by a double in situ synthesis process

Haipeng Li [a], Qiuyan Zhao [a], Baoe Li [a], Jianli Kang [b, c, *], Zhenyang Yu [b, d], Yuxiang Li [d], Xiaoqing Song [a], Chunyong Liang [a], Hongshui Wang [a]

[a] School of Materials Science and Engineering, Hebei University of Technology, Tianjin 300130, People's Republic of China
[b] State Key Laboratory of Separation Membranes and Membrane Processes, Tianjin Polytechnic University, Tianjin 300387, People's Republic of China
[c] School of Materials Science and Engineering, Tianjin Polytechnic University, Tianjin 300387, People's Republic of China
[d] School of Mechanical Engineering, Tianjin Polytechnic University, Tianjin 300387, People's Republic of China

ARTICLE INFO

Article history:
Received 5 October 2015
Received in revised form
24 January 2016
Accepted 25 January 2016
Available online 28 January 2016

ABSTRACT

Carbon nanotube (CNT)-reinforced hydroxyapatite (HA) composites were successfully fabricated by a double in situ synthesis process, which combined the in situ synthesis of CNTs in HA powders by chemical vapor deposition (CVD) with the further encapsulation of CNTs using HA by a sol–gel method. This double in situ synthesis approach not only improves the homogeneous dispersion of CNTs within the HA matrix, but also enhances the interfacial bonding between the CNTs and HA, thus leading to enhanced mechanical properties. Flexural tests indicated that the flexural strength of the composite is 1.6 times higher than that of pure HA, and significantly higher than that of the commercial and in situ synthesized CNT/HA composites. Furthermore, the in vitro cell culture experiments indicated that the CNT/HA composites fabricated by this double in situ process significantly accelerate the proliferation of fibroblast cells (L-929), compared with those fabricated by traditional methods, confirming their biocompatibility. With this biocompatibility and excellent mechanical properties, the obtained CNT/HA composites have a high potential as biomaterials, particularly in bone tissue engineering applications.

1. Introduction

Hydroxyapatite (HA) has attracted worldwide attention as an important biomaterial because of its excellent biocompatibility, osteoconductivity, and bioactivity [1,2]. However, HA is characterized by low strength and high brittleness, which hinder its widespread application. Since the discovery of carbon nanotubes (CNTs) by Iijima [3], they have been regarded as ideal reinforcement materials in composites. CNTs can significantly enhance the mechanical and physical properties of the matrix material in composites, which is attributed to the hollow structure, high aspect ratio, extraordinary strength and stiffness, and high resilience and thermal conductivity [4–7]. While CNTs have been used to enhance the mechanical properties and functional capabilities of the HA matrix [8–11], they tend to agglomerate due to their strong van der Waals interactions. Furthermore, the CNT-reinforced HA composites fabricated by traditional methods exhibit poor interfacial bonding between the CNTs and HA [12,13], resulting in a poor reinforcement efficiency.

In order to overcome these issues, some novel approaches have been proposed recently. For example, improved mechanical mixing methods such as ultrasonication and mechanical agitation/stirring have been used [14,15]. A variety of functional groups or molecules have been chemically introduced onto CNTs to improve their dispersion within the matrix using sodium dodecyl sulfate (SDS) [16–18] or a strong acid treatment [19,20], which usually introduce structural defects in the CNTs and reduce their reinforcement efficiency. Spray-drying appears to benefit the dispersion of CNTs within the HA nanoparticles [21–23]. Unfortunately, the unavoidable agglomeration of powder particles prevents the attainment of high density in some consolidation processes [14]. Recently, we proposed a novel approach, in situ chemical vapor deposition (CVD), to prepare CNT/HA composites to realize a relatively high dispersion of the intact CNTs within the HA matrix and increase the fracture toughness and flexural strength of the HA composites [24,25]. However, there are still certain challenges that limit

* Corresponding author. State Key Laboratory of Separation Membranes and Membrane Processes, Tianjin Polytechnic University, Tianjin 300387, People's Republic of China.
E-mail addresses: kangjianli@tjpu.edu.cn, jlkangnpm@126.com (J. Kang).

http://dx.doi.org/10.1016/j.carbon.2016.01.086
0008-6223/

composite performance, such as poor interfacial interactions between the CNTs and HA, which result in an unsatisfactory load transfer from the matrix to the CNTs [26]. Good interfacial bonding between the CNTs and HA matrix is needed to further enhance the mechanical properties of the composites. Furthermore, the toxicity of the uncovered CNTs in the CNT/HA composites may pose potential dangers to the human body [27,28], which must be critically assessed before their application in biomedicine.

In this study, we proposed a double in situ synthesis process to fabricate CNT/HA composites; the in situ synthesis of CNTs within the HA matrix was combined with the in situ modification of CNTs using HA. Typically, CNTs were first synthesized in situ on the HA nanoparticles by CVD using Fe catalysts. Then, a thin layer of HA was deposited in situ onto the surface of the as-grown CNT/HA composite by a sol–gel method to form HA-encapsulated CNT composite powders (CNTs@HA). These powders were then used to prepare the CNT/HA bulk composites. The double in situ synthesis approach not only improves the homogeneous dispersion of CNTs within the HA matrix, but also enhances the interfacial bonding between the CNTs and HA, leading to an increase in the flexural strength. Moreover, the complete coating of the CNTs by HA effectively prevents the former from peeling off and directly contacting the cells and tissues, thereby avoiding the effect of their potential toxicity within the human body. These CNT/HA composites have a high potential for application in biomedical implant materials.

2. Experimental

2.1. In situ synthesis of CNT/HA composite powders

Fig. 1 depicts the fabrication process of the CNT/HA composite by a double in situ synthesis process. The synthetic process of CNT/HA in situ composite powders was reported in detail in our previous study [24]. Typically, the HA nanopowders (99.0% purity, Sinopharm Chemical Reagent Co., Ltd) were added to a 0.1-mol L^{-1} $Fe(NO_3)_3 \cdot 9H_2O$ aqueous solution with constant stirring for 0.5 h, ensuring the weight ratio of Fe/HA = 5/95. Then, NaOH solution was slowly added dropwise to the above mixture with constant stirring to prepare $Fe(OH)_3$/HA colloids (Fig. 1a). The colloidal system was filtrated, washed, and calcined at 450 °C for 2 h under Ar atmosphere to produce the Fe_2O_3/HA catalyst precursor (Fig. 1b). This precursor was reduced at 700 °C under H_2 atmosphere for 1 h (Fig. 1c). Subsequently, a gaseous mixture of C_2H_2 (60 ml/min) and Ar (420 ml/min) was introduced and maintained for 1 h before cooling to room temperature under Ar protection. Finally, the in situ CNT/HA composite powders were obtained (Fig. 1d).

2.2. In situ modification of CNTs with HA

The CNT/HA powders were modified with HA by a sol–gel method. First, $Ca(NO_3)_2 \cdot 4H_2O$ and ethanol were mixed with constant stirring for 2 h. Then, P_2O_5 was dissolved in ethanol individually. After that, the $Ca(NO_3)_2$ ethanol solution was added dropwise to the P_2O_5 ethanol solution under vigorous stirring, ensuring the weight ratio of Ca/P = 5:3 and pH = 10 (Fig. 1e). The mixture was then kept at room temperature for 24 h. Then, the as-grown CNT/HA composite powders were added to the sol with constant stirring for 2 h (Fig. 1f), before being aged for 12 h. Finally, the acquired sol was dried at 80 °C for 48 h before being calcined at 450 °C for 2 h under Ar atmosphere to form the CNTs@HA powder (Fig. 1g). During this process, the mass of the acquired HA can be adjusted by changing the amount of $Ca(NO_3)_2 \cdot 4H_2O$ and P_2O_5 added. By controlling the amount of as-grown CNT/HA composite powders and

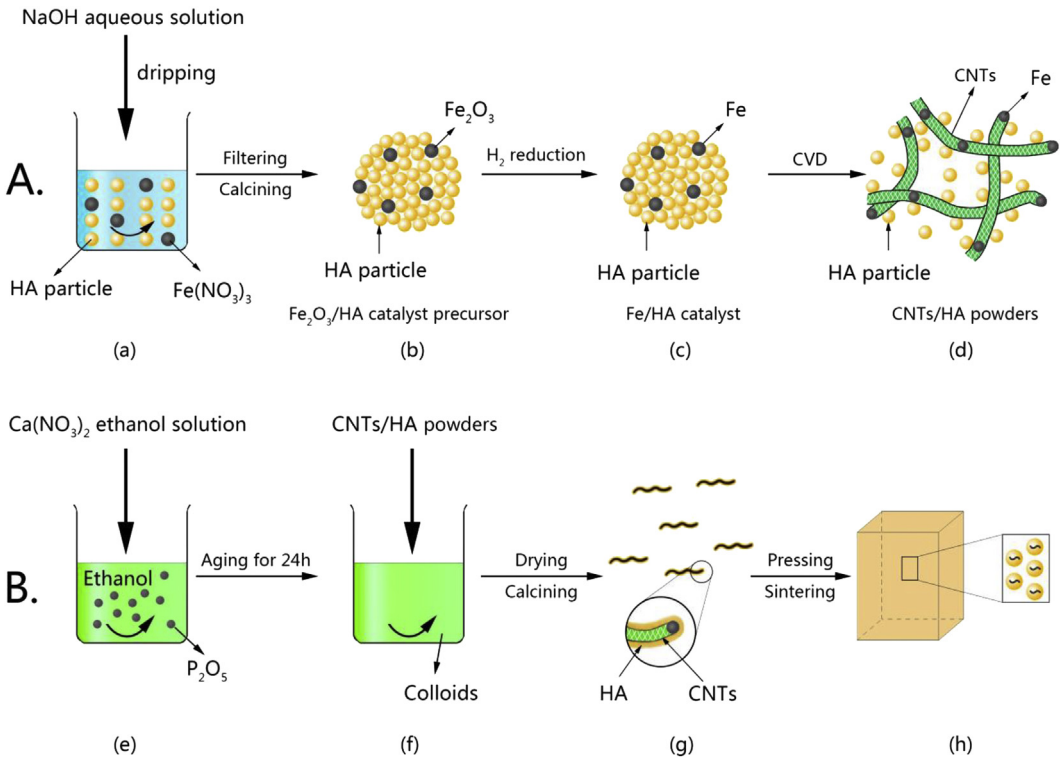

Fig. 1. Fabrication process of CNT/HA composite. (A) In situ synthesis of CNT/HA composite powders by CVD: (a) preparation of the catalyst precursor by a deposition–precipitation route, (b) formation of the Fe_2O_3/HA catalyst precursor, (c) homogeneous spread of the active Fe nanoparticles on the surface of HA powder, (d) in situ synthesis of CNTs on HA particles by CVD; (B) in situ modification of the CNTs with HA by a sol–gel method: (e) preparation of the colloids, (f) formation of the colloids by aging for 24 h, (g) formation of the CNTs@HA powder, (h) fabrication of the bulk composite by pressing and sintering. (A colour version of this figure can be viewed online.)

the mass of HA acquired during the sol–gel process, the contents of CNTs in the final CNT/HA composite powders were controlled to be approximately 1, 2, 3, and 4 wt.% (Issue 1 in Supplementary Data), which were indexed as Sample 1, 2, 3, and 4, respectively.

2.3. Preparation of CNT/HA bulk composites

The CNT/HA bulk composites were prepared by a powder metallurgy process. First, the CNT/HA composite powders were pressed in a mold under a pressure of 500 MPa. The obtained compacts were then sintered at 1100 °C for 3 h under Ar atmosphere to obtain the CNT/HA bulk composites (Fig. 1h). In addition, bulk materials made up of pure HA, commercial CNT (97.0% purity, Qinhuangdao Taiji Ring Nano-Products Co., Ltd)/HA mixtures, and in situ synthesized CNT/HA composite powders without modification were also prepared using the same process for comparison.

2.4. Cytotoxicity test

The cytotoxicity of the fabricated composites was evaluated by an in vitro cell culture test. Fibroblasts (L-929, Cell Bank of Chinese Academy of Sciences) were used to evaluate the cytocompatibility of the CNTs@HA composite powders. Cell suspension (200 μL, 1.0×10^4 cell/ml) was cocultured with the composite powders in 96-well culture plates in a humidified atmosphere of 5% CO_2 at 37 °C for 3 days. The viability of the cells on the powders was determined after 3, 24, 48, and 72 h using the inverted biological microscope (XD-202, China).

An CCK-8 [2-(2-methoxy-4-phenyl)-3-(4-phenyl)-5-(2,4-sulfo benzene)-2h-tetrazolium monosodium salt, Shanghai Yisheng Bio-Technology Co., Ltd] assay was used to quantify the cell proliferation. Briefly, fibroblast cells (L-929) were seeded into the 96-well plate at a concentration of 6000 cells per well for 24 h. The culture medium was then removed, replaced with fresh culture medium containing the samples (negative control using fragments of filter paper that are proven to be nontoxic, pure HA, the synthesized CNTs@HA, the in situ synthesized CNT/HA, and the commercial CNT/HA powders), and continuously incubated for different periods. The substrates in the wells were then discarded, and 100 μL of fresh culture medium containing 10 μL of the CCK-8 reagent was added to each well before being incubated for an additional 4 h at 37 °C. Then, the plates were gently shaken for 6 min and the absorbance was measured at 450 nm using a microplate reader (Tecan ECOM-F6124, Austria) on a spectrophotometer Spectra Count (Packard). The blank reference was taken from wells without cells that were also incubated with the CCK-8 solution. The cell viability was calculated by normalizing the optical densities (ODs) to the negative control.

2.5. Characterization

The morphology and microstructure of the CNT/HA powders and bulk composites were studied by field emission scanning electron microscopy (FE-SEM; JEOL JSM-6700F) and high-resolution transmission electron microscopy (HRTEM; Philips Tecnai G2 F20). The preparation method of the bulk TEM samples was presented in Issue 9 of Supplementary Data. X-ray diffraction (XRD; Rigaku D/Max-2500) was used to analyze the composition of the as-prepared samples. The deposition of HA onto the surface of the CNTs was characterized by zeta potential measurements (Malvern Nano-ZS90). Raman spectra were recorded on a Thermo Fisher DXR Raman microscope equipped with an Ar^+ laser with a 1064-nm line as the excitation source to validate the presence of carbon in the composite powders. FTIR spectra were recorded on a Bruker Vertex 80v spectrometer by the KBr method. The three-point bending test was performed to measure the flexural properties of the bulk samples in accordance with the ASTM C1161-13 standard. For each material, three rectangular bulk specimens of dimensions $3 \times 4 \times 45$ mm^3 were tested on 40-mm outer span three-point fixtures. Flexural tests were performed using a Shimadzu Universal Testing Machine model AG-50kNG (M/s Shimadzu, Kyoto, Japan) at room temperature with a crosshead speed of 0.5 mm/min.

3. Results and discussion

Fig. 2 shows the XRD patterns of the in situ CNT/HA composite powders and Sample 1. For the in situ CNT/HA composite powders, the low diffraction peak at $2\theta = 44.673°$ is indexed to the Fe (110) plane. The remaining peaks can be indexed to HA crystals based on their position and relative intensity. After modification with HA, the XRD pattern of Sample 1 exhibits a pattern similar to that of the in situ composite powders. No additional diffraction peaks appear, which suggests that no further crystals were formed during the modification process and the deposited HA on the surfaces of the CNTs is highly crystalline. The main diffraction peak at $2\theta = 26.6°$ associated with the graphite (002) plane [29] was not observed; this may be due to the low concentration of CNTs, which is difficult to detect by XRD.

Fig. 3 shows the typical SEM and TEM images of the in situ synthesized CNT/HA composite powders obtained by CVD. It can be seen from Fig. 3a that the CNTs, several microns in length, penetrate into the HA powders rather than growing solely on the surface. Some HA nanoclusters attached onto the surface of the CNTs to form the initial mixture of CNTs and HA. The TEM image (Fig. 3b) demonstrates that the graphitic sheets of the CNTs are apparent, and the interlayer spacing (0.342 nm) between the sheets is similar to the ideal (002) interlayer spacing (0.34 nm) of graphite. This implies the CNTs display a high degree of graphitization. Almost all of the Fe catalyst particles are at the inner sides of CNTs and tightly wrapped by the CNTs (Fig. S2). More interestingly, almost all of the HA nanoparticles attached onto the surface of the CNTs and did not peel off even under ultrasonic wave treatment during the TEM sample preparation, inferring the formation of a strong interfacial bond between the CNTs and HA during the growth of CNTs. It is well known that the matrix should possess good wettability with the reinforcing material to avoid the formation of microscale cavities

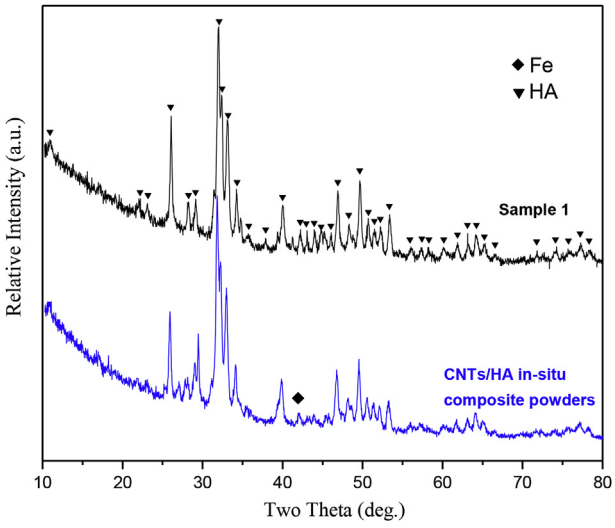

Fig. 2. XRD patterns of CNT/HA composite powders. (A colour version of this figure can be viewed online.)

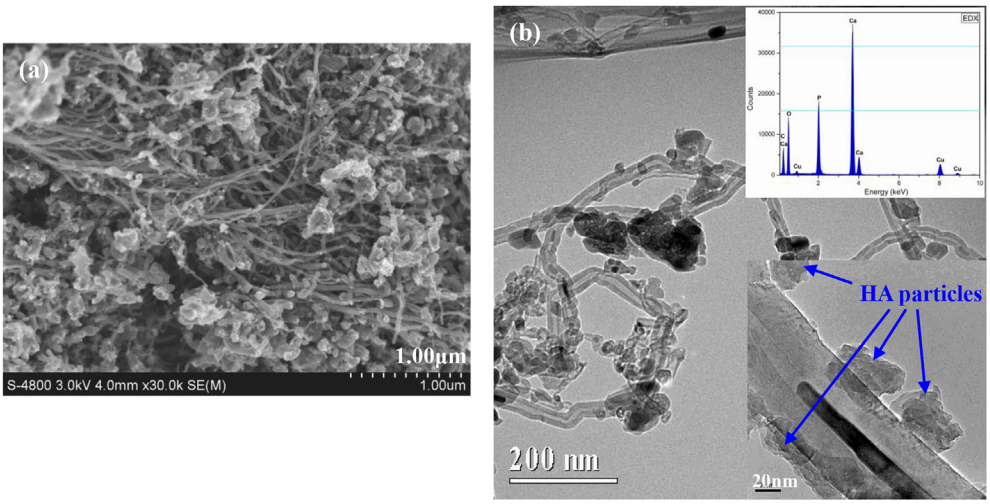

Fig. 3. (a) SEM and (b) TEM images of the in situ synthesized CNT/HA composite powders. (A colour version of this figure can be viewed online.)

and to ensure good adherence at the interface to avoid any delamination [30,31]. Being a ceramic material, HA displays poor wettability and cannot react with the CNTs. Consequently, it is difficult to generate strong bonding between the CNT reinforcements and the HA matrix by physical mixing. Therefore, the unusually strong interfacial bonding between the CNTs and HA nanoparticles in this study arises from the molecular-level contact generated by the in situ synthesis process.

During the in situ modification process, the CNTs attached by the HA nanoparticles were easily dispersed in the ethanol solution under constant stirring. At the atomic level, the precursor ions (Ca^{2+} and PO_4^{3-}) attach and react in situ on the surface of the CNTs. This results in good contact bonding between the CNTs and the obtained HA. Fig. 4 shows the SEM and TEM images of the CNT/HA composite powders after the in situ modification of the CNTs with HA. It can be seen that CNTs are completely covered by a thick HA layer. The average diameter of the CNTs increases from 30 to 70–175 nm after modification; this indicates the successful deposition of HA onto the surface of CNTs. It is worth noting that the diameter, morphology, and structure of CNTs@HA can be controlled by the amount of the in situ synthesized CNT/HA composite powders added during the modification process. When the content of CNTs in the modified system is low (Sample 1), more Ca^{2+} and PO_4^{3-} ions react on the surface of the CNTs, resulting in a more homogeneous nucleation and rapid growth of the deposited HA nanoparticles along the wall of the CNTs. Thus, the HA layer is thick and smooth, and consists of larger HA nanoparticles as shown in Fig. 4b. According to EDX (inset in Fig. 4b), the molar ratio of Ca to P is 1.623, which is close to that of HA of 1.667. The relative content of Ca^{2+} and PO_4^{3-} ions decreases with the increasing content of CNT/HA composite powders in the modified system. Thus, less HA can be formed on the surface of the CNTs. As a result, the nonhomogeneous nucleation of HA along the wall of the CNTs dominates the growth of the deposited HA nanoparticles. As shown in Fig. 4f, the HA layer becomes indented and consists of small HA nanoparticles. The interplanar spacing of the HA layer is 0.27 nm, consistent with the (300) interlayer spacing (0.272 nm) of HA. By controlling the CNT content, the thickness and morphology of the formed HA layer can be adjusted, as shown in Fig. 4g and h. Fig. 4h reveals that a thin layer with a thickness of 20 nm tightly encapsulates the CNT. The diffraction pattern (inset in Fig. 4h) confirms the existence of HA in the outer layer. The diffraction arcs in the image are ascribed to the (300), (104), (422), and (522) planes of HA. A higher magnification of the HA layer (inset in Fig. 4h) shows that the layer is composed of closely stacked, highly crystalline HA particles with a grain size of 11 nm. There is no obvious chemical reaction or new phase formed at the interface according to the HRTEM and selected area electron diffraction (SAED). The integrity of the CNTs is maintained in the composite structure, and close contact is achieved between the CNTs and the HA layer. This effectively prevents the formation of microscale cavities and ensures good adherence at the interface. Moreover, the thin HA layer acts as an intermediate layer between the CNTs and the subsequently deposited HA particles, which are indicated by arrows in Fig. 4h.

The deposition mechanism of HA onto the surface of CNTs is critical to achieve good interfacial bonding between the CNTs and HA. From Fig. 5, it can be seen that the zeta potential of the in situ synthesized CNT/HA powders varied with pH, both with and without $Ca(NO_3)_2$. The in situ synthesized CNT/HA powders are negatively charged. The addition of $Ca(NO_3)_2$ increases the measured zeta potential at all pH values studied, which indicates that the Ca^{2+} ions adsorb onto the surface of the CNTs through electrostatic attraction. Then, the PO_4^{3-} ions can react with the Ca^{2+} via electrostatic attraction to precipitate HA on the surface of the CNTs. Thus, the interfacial bonding between the CNTs and HA is electrostatic in nature, which conflicts with the previously reported chemical bonding [17,19].

Fig. 6a shows the Raman spectra of the CNT/HA composite powders before and after modification with HA. Before modification, the spectrum is dominated by two Raman bands associated with the CNTs at approximately 1347 (D band) and 1573 cm^{-1} (G band). The value of I_D/I_G is 0.70, which implies a higher graphitization degree of the in situ synthesized CNTs. After modification, the Raman peaks corresponding to the CNTs disappear, inferring that almost no CNTs were detected in the modified samples (Fig. S6a). Meanwhile, observation by TEM confirmed the presence of CNTs in the composite powders. Consequently, it is reasonable to conclude that all CNTs are completely covered by the deposited HA layers, which shield the Raman signals arising from the CNTs. Fig. 6b shows the FTIR spectra of pure HA, in situ synthesized CNT/HA and Sample 4, which further confirms the formation of CNTs@HA nanocomposites. Pure HA exhibits characteristic peaks at 561.3, 601.8, 960.5, 1037.6, 1091.6, 2850.6, and 2922.0 cm^{-1}, which is in good agreement with the literature [16]. The peaks at 561.3, 601.8, 960.5, and 1037.6 cm^{-1} are associated with the characteristic stretching and deformation vibration of the PO_4^{3-} groups [32],

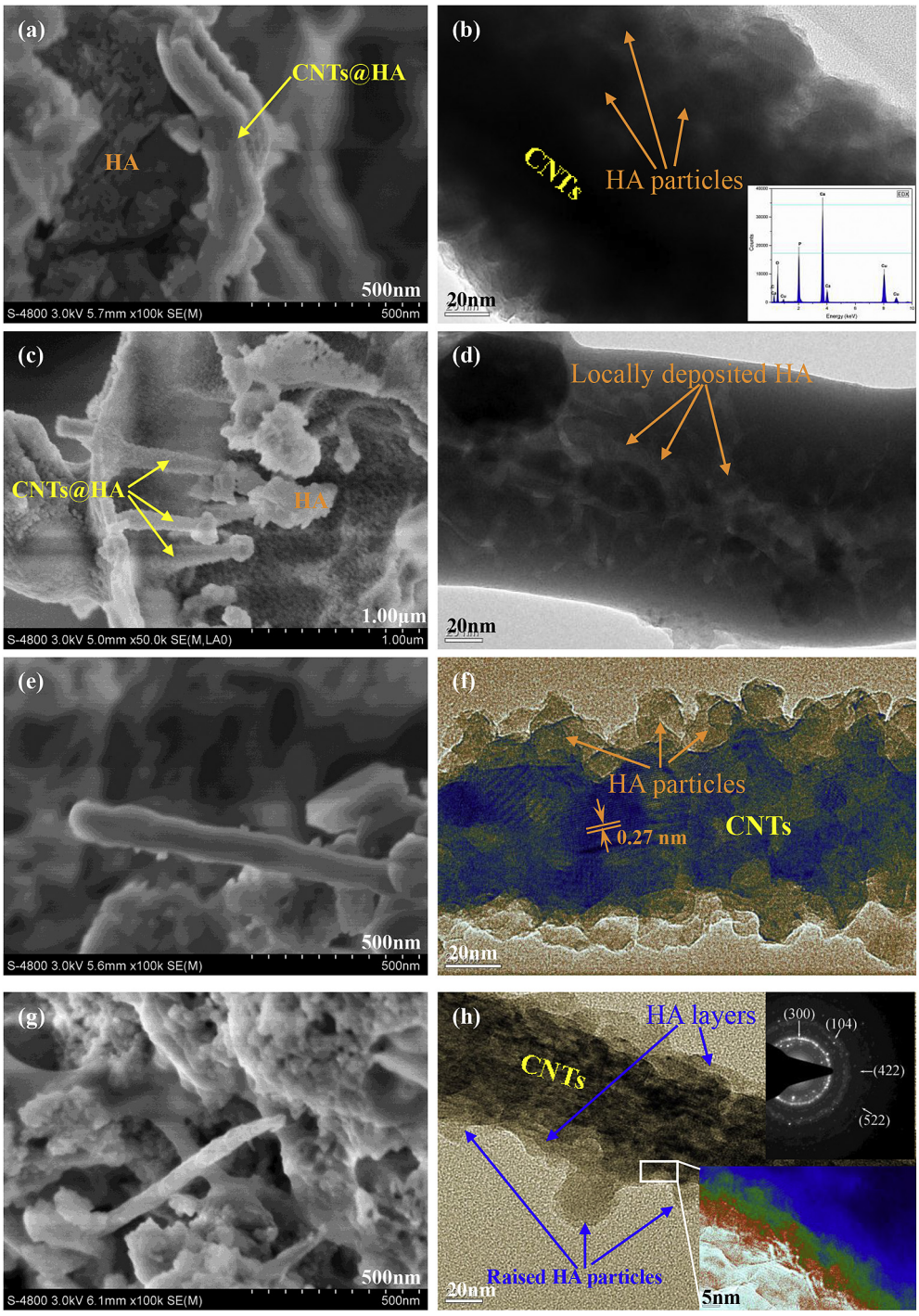

Fig. 4. SEM and TEM images of CNT/HA composite powders after modification with HA: (a, b) Sample 1, (c, d) Sample 2, (e, f) Sample 3, and (g, h) Sample 4. (A colour version of this figure can be viewed online.)

while the hydroxyl group shows characteristic peaks at 2850.6 and 2922.0 cm^{-1}. Both the in situ synthesized CNT/HA powders and the modified samples possess characteristic peaks similar to pure HA (Fig. S6b), except an additional peak at 2360.7 cm^{-1} corresponding to C═C stretching [33]. This observation confirms the presence of CNTs in the HA powders. Meanwhile, the similarities between the FTIR patterns of Sample 4 and pure HA indicate that the CNT surfaces are covered by HA through the sol–gel process.

For comparison, three types of CNT/HA bulk composites were fabricated using the same method: using commercial CNT/HA mixtures, in situ synthesized CNT/HA powders, and "double in situ" synthesized CNT/HA powders. It was found that the "double in situ" process displays improved flexural strength of the HA composite (Fig. 6c). With the addition of 3 wt.% CNTs, the flexural strength of the three composite types is maximized. The commercial and in situ synthesized CNT/HA composites display an increase of 21.15% and 42.31% over pure HA, respectively. Moreover, the flexural strength of the double in situ synthesized CNT/HA composite (Sample 3) is 83 MPa, which is 59.62% higher than that of pure HA. Meanwhile, the fracture toughness of Sample 3 is 2.4 MPa $m^{1/2}$,

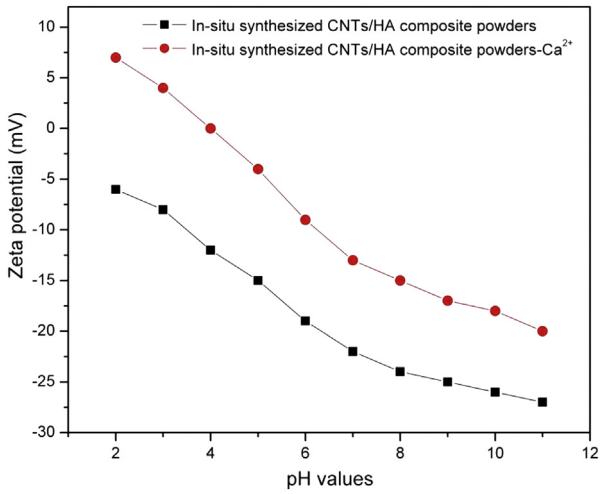

Fig. 5. Zeta potential variation with pH of the in situ synthesized CNT/HA powders with and without $Ca(NO_3)_2$. (A colour version of this figure can be viewed online.)

"double in situ" process is promising compared with the highest values reported for HA matrix composites [8,16,34].

Such excellent strengthening arises from the homogeneous dispersion and high load transfer efficiency of CNTs in the HA matrix. As shown in Fig. 7, the fracture surface of Sample 3 exhibits many dimples, implying the composite undergoes a ductile fracture [35]. Several peeled-out CNTs can be observed on the fracture surface (as shown in Fig. 7a, b and Fig. S7). It is interesting that all such CNTs are very short, which indicates that some CNTs may be broken during the fracture and thus the load transfer is high enough to break the CNTs. In addition, the good dispersion of CNTs in matrix and low porosity of the composites can also contribute to the enhancement of the mechanical properties (Table S1 and Fig. S3). The electrostatic attraction interface between the CNTs and HA that resulted in such an efficient load transfer was further confirmed by the TEM images of Sample 3. Evident lattice fringes of some of the dispersed CNTs can be observed in the HA matrix, and there are no obvious intermediate layers observed at the CNT–HA interface. These observations indicate that the bonding between the CNTs and HA are purely physical. As shown in Fig. 3, the surface

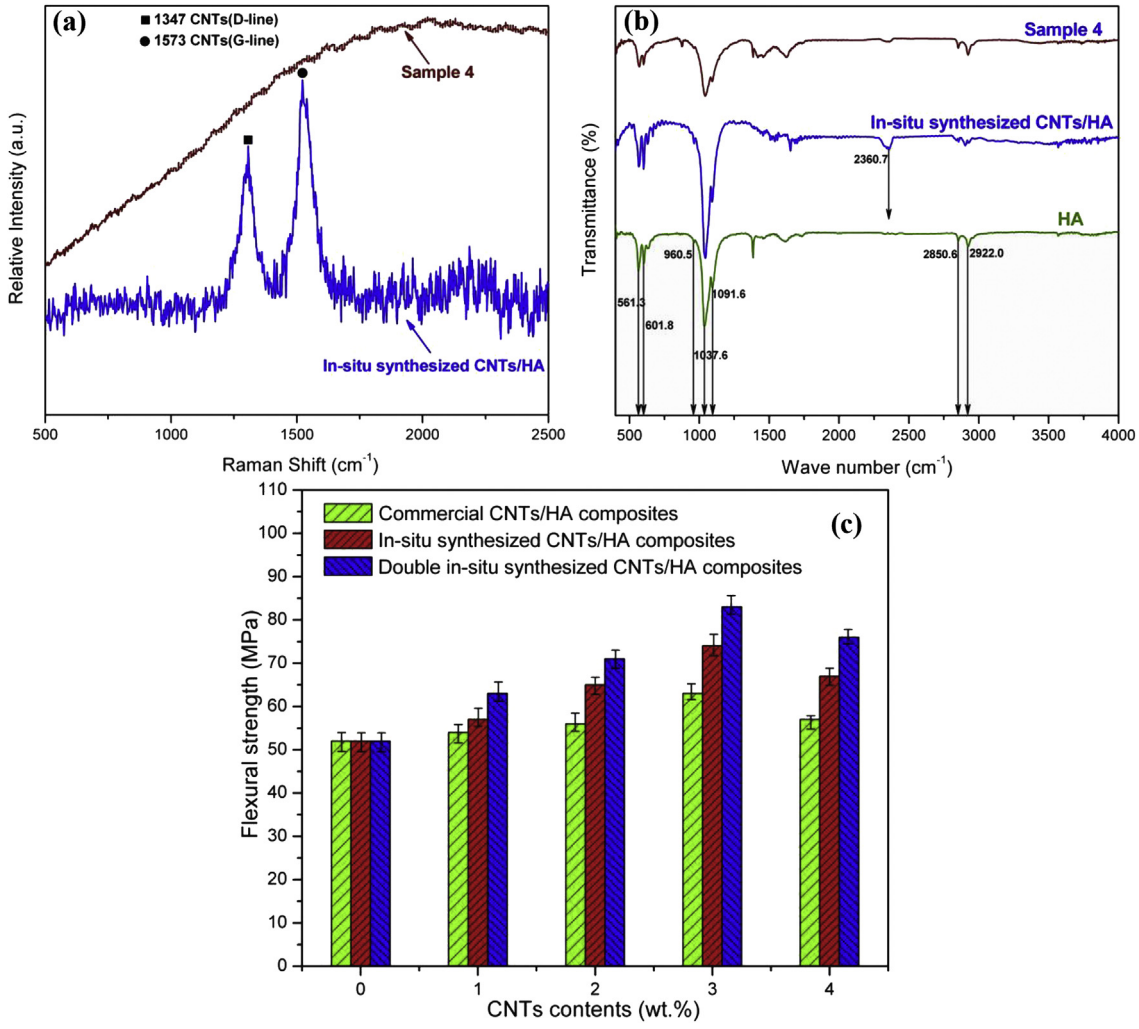

Fig. 6. (a) Raman and (b) FTIR spectra of the CNT/HA composite powders, and (c) flexural strength of pure HA and three CNT/HA composites. (A colour version of this figure can be viewed online.)

which provides a twofold improvement compared with pure HA (Fig. S4). The enhancement efficiency of these CNTs using the

of the CNTs is not uniform, and TEM observation of the composite confirms that the HA penetrates into the surface defects of the CNTs

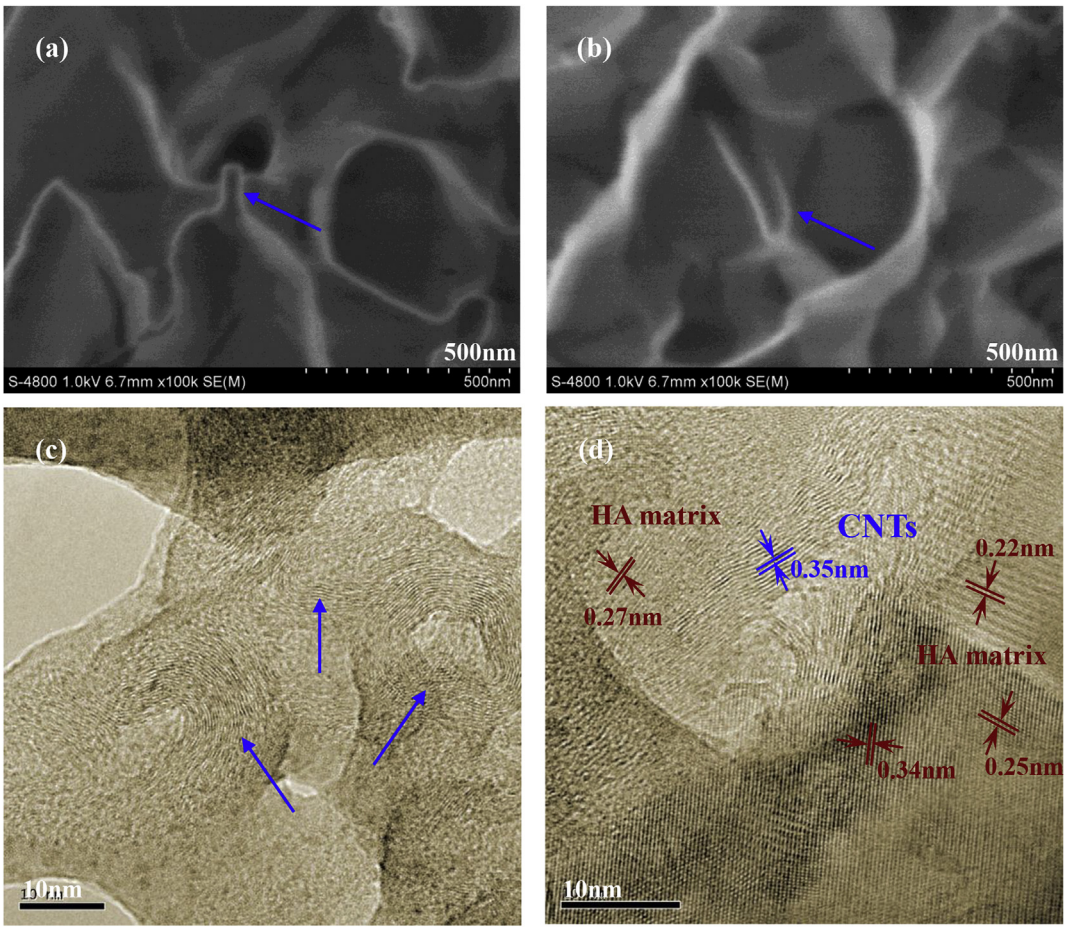

Fig. 7. (a, b) SEM images of fracture surface and (c, d) TEM images of the interface of Sample 3. (A colour version of this figure can be viewed online.)

(Fig. 7c and d) to form a strong micro-mechanical interlock. This would contribute to the high stress transfer predominantly.

In order to access the potential of the composites as biomaterials, in vitro cell culture tests were performed. Fig. 8 shows the optical images of the mouse fibroblast cells on the negative control sample, pure HA, in situ synthesized CNTs/HA, commercial CNTs/HA, and Sample 3 after culture for 48 h. It can be seen from Fig. 8c that some cells on the in situ synthesized CNTs/HA are

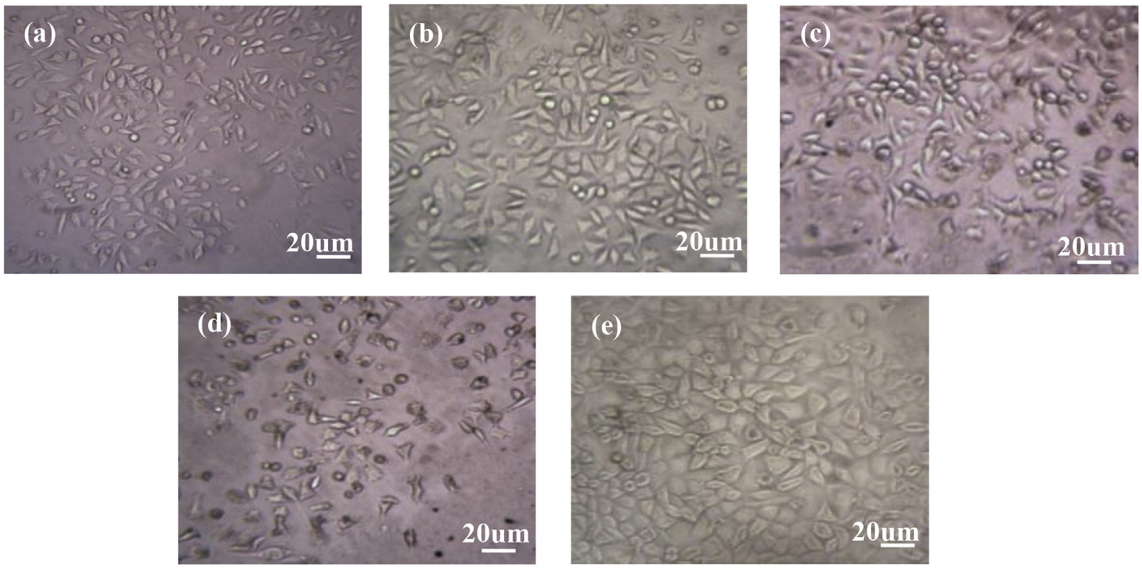

Fig. 8. Optical images of mouse fibroblast cells on the (a) negative control sample, (b) pure HA, (c) in situ synthesized CNTs/HA, (d) commercial CNTs/HA, and (e) Sample 3 after culture for 48 h. (A colour version of this figure can be viewed online.)

elliptical and have a smaller surface area. The cells on the commercial CNTs/HA, shown in Fig. 8d, exhibit a deformed morphology. In addition, the cell density on the in situ synthesized CNT/HA and commercial CNT/HA substrates is low, indicating that the in situ synthesized CNT/HA sample and commercial CNT/HA sample are cytotoxic due to the exposed CNTs, which is in good agreement with the previously reported toxicity of CNTs [36,37]. In addition, the morphologies of the cells on Sample 3 (Fig. 8e) are triangular or spindle, similar to those on the negative control sample and pure HA (Fig. 8a and b), and some cells stretch completely and are characterized by a larger surface area. This reveals that the double in situ synthesized CNTs@HA sample displays no cytotoxicity and exhibits a similar biocompatibility to pure HA. After culture for 72 h, the cell morphologies on pure HA and Sample 3 were still similar to each other (Fig. S5). Meanwhile, according to the reported in vivo studies on CNT–HA systems [34,38], the HA layers on CNTs could also make the composites more hydrophilic, and thus improve their biocompatibility.

The cell viability on the negative control sample, pure HA, Sample 3, in situ synthesized CNT/HA composite, and commercial CNT/HA composite was further evaluated by a CCK-8 assay, as shown in Fig. 9. The cell viability on the negative control sample is almost 100% as this group is nontoxic. The cell viability on pure HA maintains a value close to 96% during the incubation processes, which confirms its good biocompatibility. However, the cell viability on in situ synthesized CNT/HA and commercial CNT/HA composites decreases with the increasing exposition time, which reveals that they are cytotoxic to some extent due to the presence of exposed CNTs. On the contrary, it is interesting that the cell viability on Sample 3 increases with the culture time, achieving nearly 96%, similar to that on pure HA. In addition, the cell culture experiments were also performed using osteoblastic cells, and their results are in agreement with those from fibroblast cells (Fig. S1). Thus, the double in situ process is suitable to fabricate the CNT/HA composites with high flexural strength and good biocompatibility, showing great potential in applications such as bioimplants in the field of bone tissue engineering.

4. Conclusions

A double in situ synthesis approach was proposed to prepare HA matrix composites reinforced by CNTs, which are synthesized and modified with the help of HA nanoparticles to promote the dispersion of CNTs and the interfacial bonding between CNTs and HA. By the in situ CVD process, CNTs with a high degree of graphitization were synthesized in HA powders directly, to form a homogeneous mixture of CNTs and HA. This molecular-level contact improved the interfacial bonding and wettability between the CNTs and HA. By a sol–gel method, HA layers with good crystallinity were deposited onto the CNTs. The thickness, morphology, and structure of the deposited HA layers on the CNTs were adjustable by changing the amount of the in situ synthesized CNT/HA composite powders added during modification. TEM analysis revealed that the deposited HA layers were composed of closely stacked HA nanoparticles, and the integrity of the CNTs was maintained in the CNTs@HA composite structure. The interfacial bonding between the CNTs and HA layers was electrostatic in nature according to zeta potential measurements. Mechanical property tests showed that the double in situ process improved the flexural strength of the HA composite significantly, reaching 83 MPa, which is 1.6 times higher than that of pure HA. This improvement is due to the good dispersion and encapsulation of the CNTs in the HA matrix, as well as the strong interfacial bonding between the CNTs and HA components. Meanwhile, in vitro cell culture tests indicated that the double in situ synthesized CNT/HA composites accelerated the proliferation of the fibroblast cells (L-929) and osteoblastic cells and possessed good biocompatibility. This makes these composites promising for application in bioimplants.

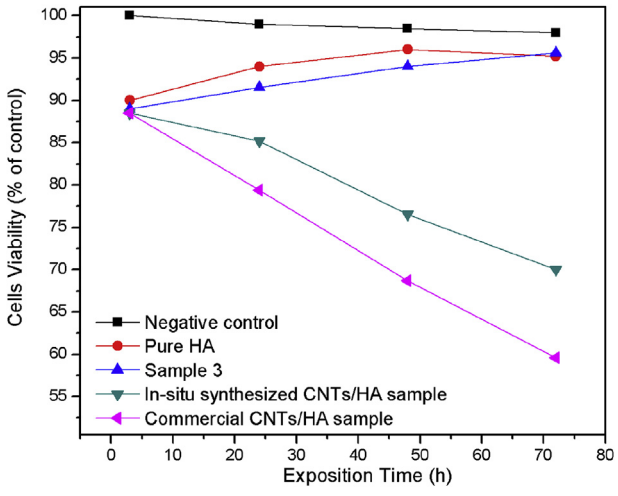

Fig. 9. Viability curve of fibroblast cells (L-929) measured by a CCK-8 assay; percentage of cell viability was calculated by normalization of ODs to negative control. (A colour version of this figure can be viewed online.)

Acknowledgments

This study was supported by the National Natural Science Foundation of China (Grant number 51201056), Natural Science Foundation of Hebei Province of China (Grant number E2015202037, E2013202021), Tianjin Research Program of Application Foundation and Advanced Technology (Grant number 14JCYBJC20900, 14JCYBJC19600), Science and Technology Correspondent Project of Tianjin (Grant number 14JCTPJC00496), and Program for Changjiang Scholars and Innovative Research Team in University of Ministry of Education of China (Grant number IRT13084).

Appendix A. Supplementary data

Supplementary data related to this article can be found at http://dx.doi.org/10.1016/j.carbon.2016.01.086.

References

[1] T. Kokubo, H.M. Kim, M. Kawashita, Novel bioactive materials with different mechanical properties, Biomaterials 24 (2003) 2161–2175.
[2] G. Muralithran, S. Ramesh, The effects of sintering temperature on the properties of hydroxyapatite, Ceram. Int. 26 (2000) 221–230.
[3] S. Iijima, Helical microtubules of graphitic carbon, Nature 354 (1991) 56–58.
[4] J. Kang, P. Nash, J. Li, C. Shi, N. Zhao, Achieving highly dispersed carbon nanofibres at high loading in carbon nanofibre-metal composites, Nanotechnology 20 (2009) 235607 (7pp).
[5] I.K. Yoon, J.Y. Hwang, J.W. Seo, W.C. Jong, H.W. Kim, U.S. Shin, Carbon nanotube-gelatin-hydroxyapatite nanohybrids with multilayer core-shell structure for mimicking natural bone, Carbon 77 (2014) 379–389.
[6] D. Mata, F.J. Oliveira, M.A. Neto, M. Belmonte, A.C. Bastos, M.A. Lopes, et al., Smart electroconductive bioactive ceramics to promote in situ electrostimulation of bone, J. Mater. Chem. B 3 (2015) 1831–1845.
[7] D. Mata, F.J. Oliveira, M. Ferro, P.S. Gomes, M.H. Fernandes, M.A. Lopes, et al., Multifunctional carbon nanotube/bioceramics modulate the directional growth and activity of osteoblastic cells, J. Biomed. Nanotechnol. 10 (2014) 725–743.
[8] A. Oyefusi, O. Olanipekun, G.M. Neelgund, D. Peterson, J.M. Stone, E. Williams, et al., Hydroxyapatite grafted carbon nanotubes and graphene nanosheets: promising bone implant materials, Spectrochim. Acta A 132 (2014) 410–416.
[9] A. Safavi, M. Sorouri, Multiwalled carbon nanotube wrapped hydroxyapatite, convenient synthesis via microwave assisted solid state metathesis, Mater.

Lett. 91 (2013) 287–290.
[10] D. Mata, F.J. Oliveira, N.M. Ferreira, R.F. Araújo, A.J.S. Fernandes, M.A. Lopes, et al., Processing strategies for smart electroconductive carbon nanotube-based bioceramic bone grafts, Nanotechnology 25 (2014) 145602 (14pp).
[11] D. Mata, A.L. Horovistiz, I. Branco, M. Ferro, N.M. Ferreira, M. Belmonte, et al., Carbon nanotubes-based bioceramic grafts for electrotherapy of bone, Mater. Sci. Eng. C 34 (2014) 360–368.
[12] S. Mukherjee, B. Kundu, S. Sen, A. Chanda, Improved properties of hydroxyapatite-carbon nanotube biocomposite: mechanical, in vitro bioactivity and biological studies, Ceram. Int. 40 (2014) 5635–5643.
[13] Y. Chen, T.H. Zhang, C.H. Gan, G. Yu, Wear studies of hydroxyapatite composite coating reinforced by carbon nanotubes, Carbon 45 (2007) 998–1004.
[14] D. Lahiri, S. Ghosh, A. Agarwal, Carbon nanotube reinforced hydroxyapatite composite for orthopedic application: a review, Mat. Sci. Eng. C 32 (2012) 1727–1758.
[15] S. Kalmodia, S. Goenka, T. Laha, D. Lahiri, B. Basu, K. Balani, Microstructure, mechanical properties, and in vitro biocompatibility of spark plasma sintered hydroxyapatite-aluminum oxide-carbon nanotube composite, Mat. Sci. Eng. C 30 (2010) 1162–1169.
[16] S. Mukherjee, B. Kundu, A. Chanda, S. Sen, Effect of functionalisation of CNT in the preparation of HAp–CNT biocomposites, Ceram. Int. 41 (2015) 3766–3774.
[17] L.P. Zhao, L. Gao, Novel in situ synthesis of MWNTs-hydroxyapatite composites, Carbon 42 (2004) 423–426.
[18] A. Abrishamchian, T. Hooshmand, M. Mohammadi, F. Najafi, Preparation and characterization of multi-walled carbon nanotube/hydroxyapatite nanocomposite film dip coated on Ti-6Al-4V by sol-gel method for biomedical applications: an in vitro study, Mat. Sci. Eng. C 33 (2013) 2002–2010.
[19] J.D. Nunez, A.M. Benito, R. Gonzalez, J. Aragon, R. Arenal, W.K. Maser, Integration and bioactivity of hydroxyapatite grown on carbon nanotubes and graphene oxide, Carbon 79 (2014) 590–604.
[20] S.C. Tsang, Y.K. Chen, P.J.F. Harris, M.L.H. Green, A simple chemical method of opening and filling carbon nanotubes, Nature 372 (1994) 159–162.
[21] D. Lahiri, A.P. Benaduce, F. Rouzaud, J. Solomon, A.K. Keshri, L. Kos, et al., Wear behavior and in vitro cytotoxicity of wear debris generated from hydroxyapatite-carbon nanotube composite coating, J. Biomed. Mater. Res. A 96A (2011) 1–12.
[22] K. Balani, R. Anderson, T. Laha, M. Andara, J. Tercero, E. Crumpler, et al., Plasma-sprayed carbon nanotube reinforced hydroxyapatite coatings and their interaction with human osteoblasts in vitro, Biomaterials 28 (2007) 618–624.
[23] D. Lahiri, V. Singh, A.K. Keshri, S. Seal, A. Agarwal, Carbon nanotube toughened hydroxyapatite by spark plasma sintering: microstructural evolution and multiscale tribological properties, Carbon 48 (2010) 3103–3120.
[24] H.P. Li, L.H. Wang, C.Y. Liang, Z.F. Wang, W.M. Zhao, Dispersion of carbon nanotubes in hydroxyapatite powder by in situ chemical vapor deposition, Mater. Sci. Eng. B 166 (2010) 19–23.
[25] H. Li, N. Zhang, X. Wang, X. Geng, X. Yang, H. Wang, et al., Synthesis and cytotoxicity of carbon nanotube/hydroxyapatite in situ composite powders prepared by chemical vapour deposition, Mater. Res. Innov. 18 (2014) 338–343.
[26] K. Hernadi, E. Ljubović, J.W. Seo, L. Forró, Synthesis of MWNT-based composite materials with inorganic coating, Acta Mater 51 (2003) 1447–1452.
[27] J. Boczkowski, S. Lanone, Respiratory toxicities of nanomaterials–A focus on carbon nanotubes, Adv. Drug Deliv. Rev. 64 (2012) 1694–1699.
[28] V. Giuseppa, P.B. Maria, I. Daniela, P. Anna, P. Alessandro, D.P. Angela, Toxicological assessment of multi-walled carbon nanotubes on A549 human lung epithelial cells, Toxicol. Vitro 29 (2015) 352–362.
[29] B.D. Hahn, J.M. Lee, D.S. Park, J.J. Choi, J. Ryu, W.H. Yoon, et al., Mechanical and in vitro biological performances of hydroxyapatite–carbon nanotube composite coatings deposited on Ti by aerosol deposition, Acta Biomater. 5 (2009) 3205–3214.
[30] R. Andrews, M.C. Weisenberger, Carbon nanotube polymer composites, Curr. Opin. Solid State Mater. Sci. 8 (2004) 31–37.
[31] T. Laha, S. Kuchibhatl, S. Seal, W. Li, A. Agarwal, Interfacial phenomena in thermally sprayed multiwalled carbon nanotube reinforced aluminum nanocomposite, Acta Mater 55 (2007) 1059–1066.
[32] M.Y. Wu, Q.Y. Wang, X.Q. Liu, H.Q. Liu, Biomimetic synthesis and characterization of carbon nanofiber/hydroxyapatite composite scaffolds, Carbon 51 (2013) 335–345.
[33] M.K. Kumar, A.L.M. Reddy, S. Ramaprabhu, Exfoliated single-walled carbon nanotube-based hydrogen sensor, Sens. Actuat. B 130 (2008) 653–660.
[34] A.M. Li, K.N. Sun, W.F. Dong, D.M. Zhao, Mechanical properties, microstructure and histocompatibility of MWCNTs/HAp biocomposites, Mater. Lett. 61 (2007) 1839–1844.
[35] A. Das, S. Tarafder, Geometry of dimples and its correlation with mechanical properties in austenitic stainless steel, Scr. Mater 59 (2008) 1014–1017.
[36] D.X. Cui, F.R. Tian, C.S. Ozkan, M. Wang, H.J. Gao, Effect of single wall carbon nanotubes on human HEK293 cells, Toxicol. Lett. 155 (2005) 73–85.
[37] L.H. Ding, J. Stilwell, T.T. Zhang, O. Elboudwarej, H.J. Jiang, J.P. Selegue, et al., Molecular characterization of the cytotoxic mechanism of multiwall carbon nanotubes and nano-onions on human skin fibroblast, Nano Lett. 5 (2005) 2448–2464.
[38] S. Facca, D. Lahiri, F. Fioretti, N. Messadeq, D. Mainard, N. Benkirane-Jessel, et al., In vivo osseointegration of nano-designed composite coatings on titanium implants, ACS Nano 5 (2011) 4790–4799.